



## Self-assembly of flagellin on Au(111) surfaces



Alejandro González Orive<sup>a</sup>, Diego E. Pissinis<sup>b</sup>, Carolina Díaz<sup>b</sup>, Alejandro Miñán<sup>b</sup>, Guillermo A. Benítez<sup>b</sup>, Aldo Rubert<sup>b</sup>, Antonieta Daza Millone<sup>b</sup>, Martín Rumbo<sup>c</sup>, Alberto Hernández Creus<sup>a</sup>, Roberto C. Salvarezza<sup>b</sup>, Patricia L. Schilardi<sup>b,\*</sup>

<sup>a</sup> Unidad de Química Física, Departamento de Química, Facultad de Química, Instituto Universitario de Materiales y Nanotecnología (IMN), Universidad de La Laguna, Avda. Francisco Sánchez, s/n, 38071-La Laguna, Tenerife, Spain

<sup>b</sup> Instituto de Investigaciones Físicoquímicas Teóricas y Aplicadas (INIFTA), CONICET – Departamento de Química, Facultad de Ciencias Exactas, Universidad Nacional de La Plata, CC16, Suc. 4, La Plata, Buenos Aires, Argentina

<sup>c</sup> Laboratorio de Inmunología, Facultad de Ciencias Exactas, Universidad Nacional de La Plata, 47 y 115, La Plata, Buenos Aires, Argentina

### ARTICLE INFO

#### Article history:

Received 7 April 2014

Accepted 8 July 2014

Available online 18 July 2014

#### Keywords:

Flagellin

Self-assembly

Protein adsorption

Cytochrome C

### ABSTRACT

The adsorption of flagellin monomers from *Pseudomonas fluorescens* on Au(111) has been studied by Atomic Force Microscopy (AFM), Scanning Tunneling Microscopy (STM), X-ray Photoelectron Spectroscopy (XPS), Surface Plasmon Resonance (SPR), and electrochemical techniques. Results show that flagellin monomers spontaneously self-assemble forming a monolayer thick protein film bounded to the Au surface by the more hydrophobic subunit and exposed to the environment the hydrophilic subunit. The films are conductive and allow allocation of electrochemically active cytochrome C. The self-assembled films could be used as biological platforms to build 3D complex molecular structures on planar metal surfaces and to functionalize metal nanoparticles.

© 2014 Elsevier Inc. All rights reserved.

## 1. Introduction

Protein interaction with metal surfaces raises fundamental questions regarding their binding tendency, their distribution on the surface, as well as the occurrence of adsorption-induced conformational modifications which may change their biological properties; addressing these questions, and being able to tune protein–surface interactions, is of primary importance for the control of biointerfaces. In particular, protein–surface interactions have great significance in many applications ranging from nanotechnology to medicine. In fact, protein immobilization on surfaces has important applications in drug screening, biosensing, bioassaying, and protein characterization.

Fundamental interactions between proteins and solid surfaces include one or a combination of the following processes: physical adsorption, electrostatic forces, specific recognition and covalent binding [1]. These interactions depend sensitively upon the local structures and environment of protein binding sites on surfaces.

Flagellin is a globular protein that assembles itself in forming a hollow cylinder structure that constitutes the bacterial flagella. Flagellin from *Salmonella* has been extensively studied as a

prototypical member of this family. This protein contains well-folded protein domains and intrinsically disordered regions [2]. Electron cryomicroscopy and X-ray diffraction studies [3,4] have revealed the complex subunit structure within the filament. Polymeric flagellin consists of four linearly connected domains labeled D0, D1, D2, and D3, which are arranged from the inside to the outside of the filament. While D0 and D1 domains are highly conserved along different bacterial species, D2 and D3 domain show high variability [5]. The disordered terminal regions are involved in D0 and partly in D1, forming long helical bundles, and their direct interaction is responsible for stabilizing the filament structure. The segment involving D2 and D3, is exposed on the surface of flagellar filaments. D3 is a structurally independent part of flagellin; it is not essential for filament formation [3].

The D3 domain has been proposed as a good target for genetic engineering studies. Substituting the central D3 domain by an appropriate artificial peptide sequence can give flagellin analyte affinity sensing or enzymatic properties [4,6]. Recently, the incorporation of green fluorescent protein (GFP) was also demonstrated [7]. The easy formation of compact, stable, well ordered and oriented functional layers can facilitate the development of these directions. Thus, flagellin can have interesting applications in chemical or biological sensing, medical diagnostic, environmental monitoring, as well as in nanobiotechnology and nanomedicine. On this regard, it has been reported that flagellin is able to increase

\* Corresponding author. Address: INIFTA, CC16 Suc. 4, 1900 La Plata, Buenos Aires, Argentina. Fax: +54 221 4254642.

E-mail addresses: [pls@inifta.unlp.edu.ar](mailto:pls@inifta.unlp.edu.ar), [pls@quimica.unlp.edu.ar](mailto:pls@quimica.unlp.edu.ar) (P.L. Schilardi).

the immune response, either *in vitro* or *in vivo*, after systemic administration [8]. For instance, the recombinant flagellin–ovalbumin fusion protein induces both, humoral and cell-based immunity of mice [9]. Thereby, biocompatible calcium phosphate nanoparticles functionalized with flagellin have been tested as adjuvant in vaccination, resulting in an enhanced immunostimulation [10]. Flagellin-coated bioadhesive poly(anhydride) nanoparticles have also been investigated as possible strategy in oral vaccination, resulting in a strong long lasting systemic and mucosal immune responses than the respective non-conjugated vectors [11]. On the other hand, metallic nanoparticles, and particularly gold nanoparticles, are being widely studied in relation to their biological applications, such as cancer diagnostics and therapy, drug delivery and vaccine preparation, among others [12]. Along this line, the possibility of immobilizing flagellin on gold, as well as the elucidation of the spatial structure of the protein layer, opens the opportunity of modifying the surface of metallic nanoparticles and design useful systems for biomedical applications.

Otherwise, the structure of flagellin thin films adsorbed on highly hydrophobic (silanized)  $\text{SiO}_2/\text{TiO}_2$  planar substrates has been recently elucidated [13]. Thus, the potential applications of flagellin-modified electrical conducting metal surfaces can be extended to electroanalytical techniques on the fields mentioned above.

## 2. Experimental

### 2.1. Bacterial culture

*P. fluorescens* strain, kindly provided by Dr. Christine Gaylarde (Department of Biology and Chemistry, UNIJUI, RS, Brazil) was identified by standard bacteriological tests using selective growth media and biochemical tests. This strain was maintained as inoculated slant in Cetrimide Agar (DIFCO) at 28 °C. The slant was incubated under conditions allowing microbial growth and then stored in a refrigerator at a temperature below the minimum required for culture growth. Passages of the stock were performed every 20 days. The inoculum was prepared by suspending a Cetrimide agar slant (24 h old) in 2 mL sterile Nutrient Broth for microbiology (MERCK). The inoculum was poured into an Erlenmeyer flask containing 300 mL nutrient broth medium and kept on a rotary shaker overnight at 28 °C. Following incubation, the bacterial suspension was adjusted to  $10^8$  colony-forming units (CFU)  $\text{mL}^{-1}$  in fresh growth medium which was confirmed by viable count method. It is worth to mention that our studies were conducted without gene modification of the strain.

### 2.2. Flagella and flagellin isolation

Flagella and flagellin isolation was adapted from the purification protocol described by Hiriart et al. [14]. Briefly, 1 mL of bacteria suspension ( $10^8$  CFU  $\text{mL}^{-1}$ ) was used to inoculate 1 L of nutrient broth. This culture was aerated in a glass laboratory bioreactor for 24 h at 30 °C, with an air flow rate of 10 L/min without agitation to avoid mechanical deflagellation.

One litre of bacterial culture prepared in the bioreactor was centrifuged (Biofuge 22R, Heraeus Sepatech, Germany) at 6500 rev/min for 30 min at 4 °C. The cell pellet was suspended in 18 mL of phosphate buffer saline dissolution (PBS) (10 mM, pH 7.0) and submitted to flagellin extraction by shear using vortex agitation for 10 min at 40 Hz (VELP Scientifica, Europe). After shearing, bacterial pellet was obtained by centrifugation at 14,000 rev/min for 15 min. The collected supernatant was then submitted to ultracentrifugation (35,000 rev/min for 2 h at 4 °C, in a Beckman ultracentrifuge) to obtain the flagellar pellet. Finally the flagellar pellet was

resuspended in 2 mL of saline solution and then incubated in a 70 °C water bath for 20 min to obtain flagellin in monomeric form. The final concentration of the dissolution was 0.05 mg/mL, determined by the bicinchoninic acid (BCA) method using albumin as standard, following manufacturer's indications (Pierce, CA, USA).

### 2.3. Sample preparation

Gold substrates consisted in a thin layer of gold deposited on glass and were purchased from Arrandee® (Germany). The substrates were annealed in butane flame in order to obtain (111) terraces and then immersed in the flagellin-containing dissolution diluted 1:10 with phosphate buffer dissolution (PB) 10 mM, pH 7.3 at 4 °C. After 24 h the samples were gently rinsed with PB and dried for 48 h at 4 °C on a desiccant cushion. This procedure allowed us to obtain a thin layer of protein. Thick layers of flagellin on gold were obtained by drop casting 40  $\mu\text{L}$  of the flagellin-containing dissolution (in such a way that the entire electrode was covered) and dried at 4 °C. Horse heart cytochrome C (Cyt C) (Aldrich) 99.9% was used as received. Cyt C adsorption on flagellin was carried out by immersing the flagellin-modified gold substrate in a 1 mg/mL of Cyt C in 1 mM (pH = 7.3) PB dissolution for 30 min. The samples were rinsed with the 1 mM PB dissolution and dried in air. Occasionally, the flagellin self-assembly was performed on nanometer-sized polycrystalline Au. The roughness (measured as root mean square, rms) of the polycrystalline substrate used for AFM imaging is 2–3 nm, similar to those measured for the SPR substrates, which resulted in 2.5 nm.

### 2.4. AFM and STM imaging

AFM imaging was made in air with a Nanoscope V microscope from Digital Instruments operating in tapping mode. Images were taken at a scanning rate of 1 Hz with etched silicon tips (RTESP, 215–254 kHz and 20–80 N/m). AFM was also used to estimate the protein film thickness by repetitive scanning the sample with the AFM tip. In this case a silicon nitride probe with a spring constant of 0.4950 N/m was used applying 134 nN load in air. This load was sufficient to open a window by removing the protein from the surface without damage of the underlying substrate. The cross section analysis of the window allows an estimation of the film thickness.

Structural data and electronic properties of the flagellin films were also determined by Scanning Tunneling Microscopy (STM) and scanning tunneling spectroscopy (STS), respectively, using a Nanoscope E STM (Digital Instruments) operating in air at room temperature. Pt–Ir tips were used for these measurements. The tunneling current vs bias voltage ( $I$  vs  $V$ ) curves were obtained by averaging over at least five different regions of the samples.  $I/E$  data shown in this paper are the averaged result of around 400  $I/E$  curves collected in each zone.

### 2.5. Electrochemical measurements

Electrochemical measurements were performed in a three-electrode electrochemical cell; substrates prepared as described above were used as working electrode (counterelectrode: platinum foil, reference electrode: saturated calomel electrode, SCE). The electrolyte dissolution was PB 10 mM (pH = 7.3). The sweep rate was 100 mV/s. Voltammograms were recorded by using a Voltalab or Teq galvanostat-potentiostat.

### 2.6. X-ray Photoelectron Spectroscopy (XPS)

XPS measurements were performed using a Mg  $K\alpha$  source (XR50, Specs GmbH) and a hemispherical electron energy analyzer

(PHOIBOS 100, Specs GmbH) operating at 40 eV pass energy. A two-point calibration of the energy scale was performed using sputtered gold and copper samples (Au 4f<sub>7/2</sub> binding energy (BE) = 84.00 eV; Cu 2p<sub>3/2</sub> BE = 932.67 eV). C 1s at 285 eV was used as charging reference.

2.7. SPR measurements

Adsorption of flagellin on a bare gold surface was measured in scanning angle mode of SPR Navi™ 200 (BioNavis, Tampere, Finland) with a 670 nm laser. SPR Navi™ Gold sensors (50 nm thickness of gold evaporated on glass slides) were cleaned with NH<sub>3</sub>:H<sub>2</sub>O<sub>2</sub> 1:1 solution prior to use. PB (10 mM) flow rate was kept at 10 μL/min and after a baseline was achieved, flagellin solution (50 μg/mL in PB) was injected at same flow rate. Measurements were made in duplicate in parallel channels. The surface concentration (surface mass density) was calculated by the de Feijter equation [15] (Eq. (1))

$$\Gamma_p = \frac{(n_p - n_m)d_p}{d_n/d_c} \tag{1}$$

where  $n_p$  is the refractive index (RI) of the protein monolayer,  $n_m$  is the medium RI,  $d_p$  the sample layer thickness and  $d_n/d_c$  the RI (mass) concentration dependency.

The instrument signal is included by the expression  $n_p - n_m = \Delta n = \Delta\theta \cdot k$ . Thus,

$$\Gamma_p = \frac{\Delta\theta \cdot k \cdot d_p}{d_n/d_c} \tag{2}$$

where the constant  $k$  is the instrument (sensor, wavelength) dependent coefficient for sensitivity, and  $\theta$  is the angular response in the measurement. For thin layers (<100 nm) the  $k \cdot d_p$  term can be considered constant. For SPR Navi 200, the  $k \cdot d_p$  values in water based buffers and Au based sensors is  $1.0 \times 10^{-7}$  nm/deg at 670 nm. In the calculation, we considered  $d_n/d_c = 0.189$  cm<sup>3</sup>/g for flagellin [13].

3. Results and discussion

XPS data of Au samples after immersion in the flagellin containing solution for 24 h (Fig. 1) indicates that the protein monomers spontaneously adsorb on the substrate. In fact, the survey spectrum shows the presence of C, N, O and P peaks on the Au sample (Fig. 1a). The high resolution spectrum of N 1s core level (Fig. 1b) shows two components centered at ≈399.9 eV and ≈400.9 eV which have been assigned to the unprotonated and protonated amine/amide species, respectively present in aminoacids [16,17] and protein molecules [18] adsorbed on Au. On the other hand, the C 1s spectrum is resolved into four components (Fig. 1c). The component at ≈285 eV corresponds to C–C and C–H, the component at ≈286.5 eV is assigned to carbon bound to nitrogen (C–N) and hydroxyl groups (C–OH), the component at ≈287.9 eV corresponds to carbonyl groups (aldehydic or ketonic carbon), and the high binding energy component at ≈288.7 eV is attributed to carboxylate (O=C–O<sup>-</sup>) and amide carbon (N–C=O). The small P 2p signal (Fig. 1a) has been related to phosphate bound to *Pseudomonas* flagellin [19]. Finally, the large O 1s peak in Fig. 1a is consistent with the presence of the adsorbed protein and physisorbed water in the film. The presence of the Au peak in the XPS spectra (Fig. 1a) indicates that the flagellin film is relatively thin and/or discontinuous allowing detection of photoelectrons coming from the substrate.

On the other hand, contact angle measurements on these films yield ≈40° revealing that the surface of the adsorbed protein film is hydrophilic. Control experiments made using the uncovered Au

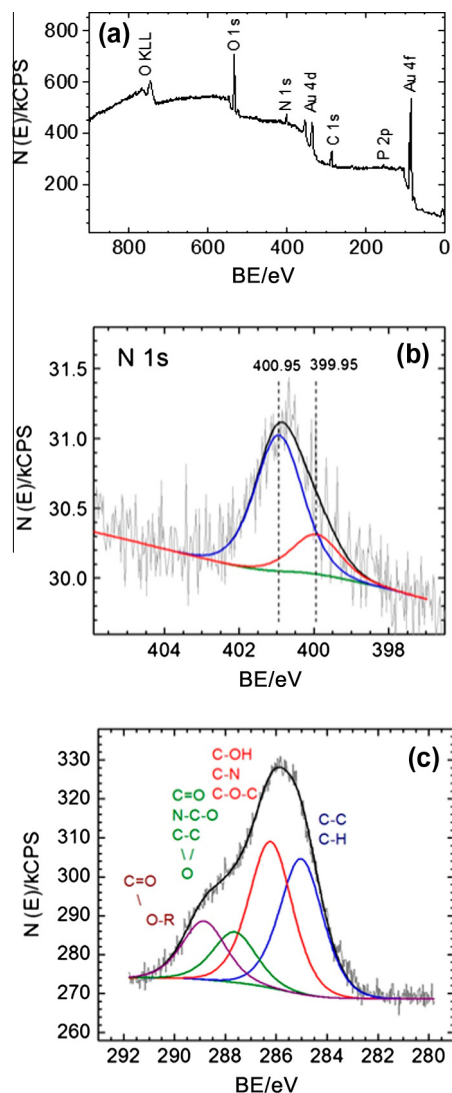


Fig. 1. XPS spectra of flagellin adsorbed on Au. (a) Survey spectrum; (b) N 1s core level. (c) C 1s core level. (For interpretation of the references to color in this figure, the reader is referred to the web version of this article.)

substrate after flame annealing and dodecanethiol covered Au results in 60° and 90°, respectively.

Quantitative information about the adsorption of flagellin on the Au surface can be obtained by the SPR measurements. The sensorgram revealed that flagellin has a fast adsorption kinetic on the substrate reaching saturation for adsorption times  $t > 20$  min (Fig. 2). After the weakly adsorbed protein is removed by flowing buffer dissolution, a final change  $\Delta\theta = 0.1328$  deg was obtained. Thus, by using Eq. (2), the surface density of the flagellin monolayer adsorbed on the Au surface results in 70.2 ng cm<sup>-2</sup>.

We have used AFM to study the structure of the flagellin film. Fig. 3a shows a typical topographic AFM image of the adsorbed layer which consists of rounded units (bright regions) and pores (dark regions), as can be seen in more detail in the inset. The power spectral density (PSD) of the AFM images gives two characteristic lengths at ≈8 and ≈14 nm, respectively (Fig. 3b). We assign the first length to the average size of the rounded units and the second length to the average pore size. Therefore, by considering the average pore and unit sizes the pores should be delimited by 4–6 close packed units. Similar results were obtained using Au substrates with nanometer-sized grains. We have also estimated the thickness of the adsorbed protein layer by opening a window by

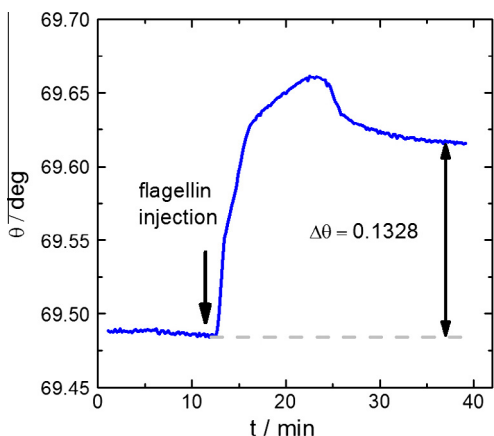


Fig. 2. SPR sensorgram of flagellin adsorption on Au (PB flow rate of 10  $\mu\text{L}/\text{min}$ ).

repetitive scanning the AFM tip at a relatively high applied force over a preset area of the sample (Fig. 3c). The cross section analysis of the window reveals that the film thickness is  $\approx 7 \text{ nm} \pm 1 \text{ nm}$  (Fig. 3d).

The flagellin layer can be also imaged by STM (Fig. 3e) indicating that the film is conductive [20], and mechanically stable under the scanning of the STM tip as well. As can be seen in Fig. 3e, the surface features imaged by STM are similar to those observed by AFM imaging (Fig. 3a). However, the statistical analysis of the STM data results in  $\approx 5 \text{ nm}$  average size for the rounded units and a bimodal distribution with average sizes centered at  $\approx 7$  and  $\approx 12 \text{ nm}$  for the pores nm (Fig. 3f). We associate the 5 nm and 12 nm nm features shown in STM images with the 8 nm and 14 nm features observed in the AFM images, while the 7 nm pore size detected in STM should be included in the 8 nm peak in the AFM PSD. The sharper STM tip allows a better resolution than the AFM tip, showing in greater detail the complex pore structure (Fig. 3e inset).

It is worth noting that STM imaging is only possible if electron tunneling is allowed. We have further explored the electrical properties of our films by STS. Typical curves of tunneling current ( $I$ ) vs. bias voltage ( $V$ ) for Au(111), and for the different regions of the flagellin layer are shown in Fig. 4. The  $I/V$  curve for the bare substrate shows an almost linear behavior, as expected for metallic conductors (Fig. 4a) [21]. A similar response can be observed when the tip is located on the pores of the protein layer (Fig. 4b). In contrast,  $I/V$  curves collected on top of the rounded units are nonlinear as shown in Fig. 4c. The conductivity of the flagellin films could be explained by different contributions such as direct tunneling from the tip to the Au substrate through a thin non-conductive biological film, electron transport through the peptides subunits, and proton/ion conduction under the applied field. The latter has been proposed to explain STM images of biological materials such as DNA when covered by a very thin water layer [22]. Also water molecules and ions can be adsorbed at the hydrophilic protein pockets. Elucidation of the mechanisms involved in flagellin film conductivity is an interesting topic that deserves further experimental and theoretical work.

We have also analyzed the electrochemical behavior of the protein film. A typical voltammogram recorded for the adsorbed flagellin film on Au in the PB solution is shown in Fig. 5. The adsorbed protein inhibits the gold oxide formation at positive potentials, and the capacitance of the electrochemical double layer is reduced after immersion in the protein dissolution (Fig. 5). A similar response has been observed for the adsorption of different proteins on gold surfaces [23,24]. No peaks related to charge transfer reactions can be observed in the potential window analyzed, i.e. no redox groups are present in the protein film. Note, however,

that the transport of ions and water is only partially blocked as revealed by the relatively high double layer capacitance when compared to that observed for a self-assembled monolayer of mercaptoundecanoic acid (MUA) (Fig. 5). It is well known that alkanethiol molecules adsorb on gold surfaces forming crystalline and ordered structures films stabilized by lateral interactions that block the transport of water and ions to the metal surface. Thus, the discontinuities and the porous structure of the flagellin film (see Fig. 6 below) that leave some regions of the gold substrate uncovered seems to be the origin of the relative high double layer capacitance mentioned above.

The experimental data give evidence on the structure of the adsorbed protein. It has been shown that the overall shape of the flagellin monomer approaches the shape of an upper case Greek gamma with a long arm of  $\approx 14 \text{ nm}$  and a shorted one of  $\approx 11 \text{ nm}$  [25]. The longer arm is composed by domains D0, D1, while the shorter one is formed by the domains D2 and D3. These domains exhibit different hydrophilic/hydrophobic features. The analysis of the structure of flagellin by electron cryomicroscopy revealed that D0 domain includes  $\alpha$ -helical coils, while D1 involve  $\alpha$ -helical coils and  $\beta$ -hairpins [26]. In terms of interactions, hydrophobic forces mediate between the D0 domain and other subunits, whereas those of the D1 domain involve polar–polar or charge–polar interactions [27]. Domains D2 and D3 consist of mainly  $\beta$ -strands. D3 is connected to D2 via a pair of short antiparallel beta-strands and comprises the most stable part of monomeric flagellin playing an important role in the stabilization of the other two (D1 and D2) domains [3].

It has been recently shown [13] that flagellin molecules only adsorb on hydrophobic surfaces by the hydrophobic, disordered [28], and flexible [25] D0 domain placed at the terminal portion of the long arm. Flexibility is an important factor for protein adsorption on Au surfaces [29]. On the other hand, large molecules with planar  $sp^2$  hybridized groups such as Arg, Gln, Tyr, present in D0 adsorb strongly on Au surfaces by the N-containing and carboxylate groups [30]. Therefore, we expect that flagellin adsorb by the terminal hydrophobic D0 domain with the longer arm (nearly parallel to the Au surface), and exposing the more hydrophilic D3 subunit of the shorter arm (nearly vertical to the Au surface) to the environment (Fig. 6a). The assembly of the protein to form the film should not only involve the interaction of the N-containing and carboxylate groups of the aminoacids present in the D0 domains with the Au surface but also hydrogen bonding and electrostatic interactions between the different functional groups belonging to the aminoacids of D1, D2 and D3 domains from adjacent molecules. The inner/hydrophobic outer/hydrophilic configuration of the film is consistent with the hindering of the gold oxide monolayer formation observed in the electrochemical profiles as a hydrophobic inner layer makes difficult the access of  $\text{OH}^-$  ions and water molecules needed to form the gold oxide. On the other hand the external hydrophilic D3 domain explains the  $40^\circ$  contact angle measured on these films.

Now we turn on the structure of the flagellin film. Considering that the adsorbed mass of flagellin is  $70.2 \text{ ng cm}^{-2}$  and the molecular weight of *P. fluorescens* is 48.6 kDa [31] a cylindrical-like structure having 14 nm in radius should involve 4–6 flagellin units, in good agreement with the AFM and STM measurements. Then, we propose that 4–6 flagellin monomers self-assembly by hydrogen bonding and electrostatic interactions (D2 and D3) and hydrophobic interactions (D0 and D1) in a cylindrical-like structure, as shown in Fig. 6b.

This model reasonably explains the primary structure of the film observed by STM that consist of rounded units 5 nm in average size (the projection of the D2 and D3 domains to the surface) organized around a large pore 12 nm in size (the exposed regions of the D0 and D1 arms at the film bottom). The organization of this

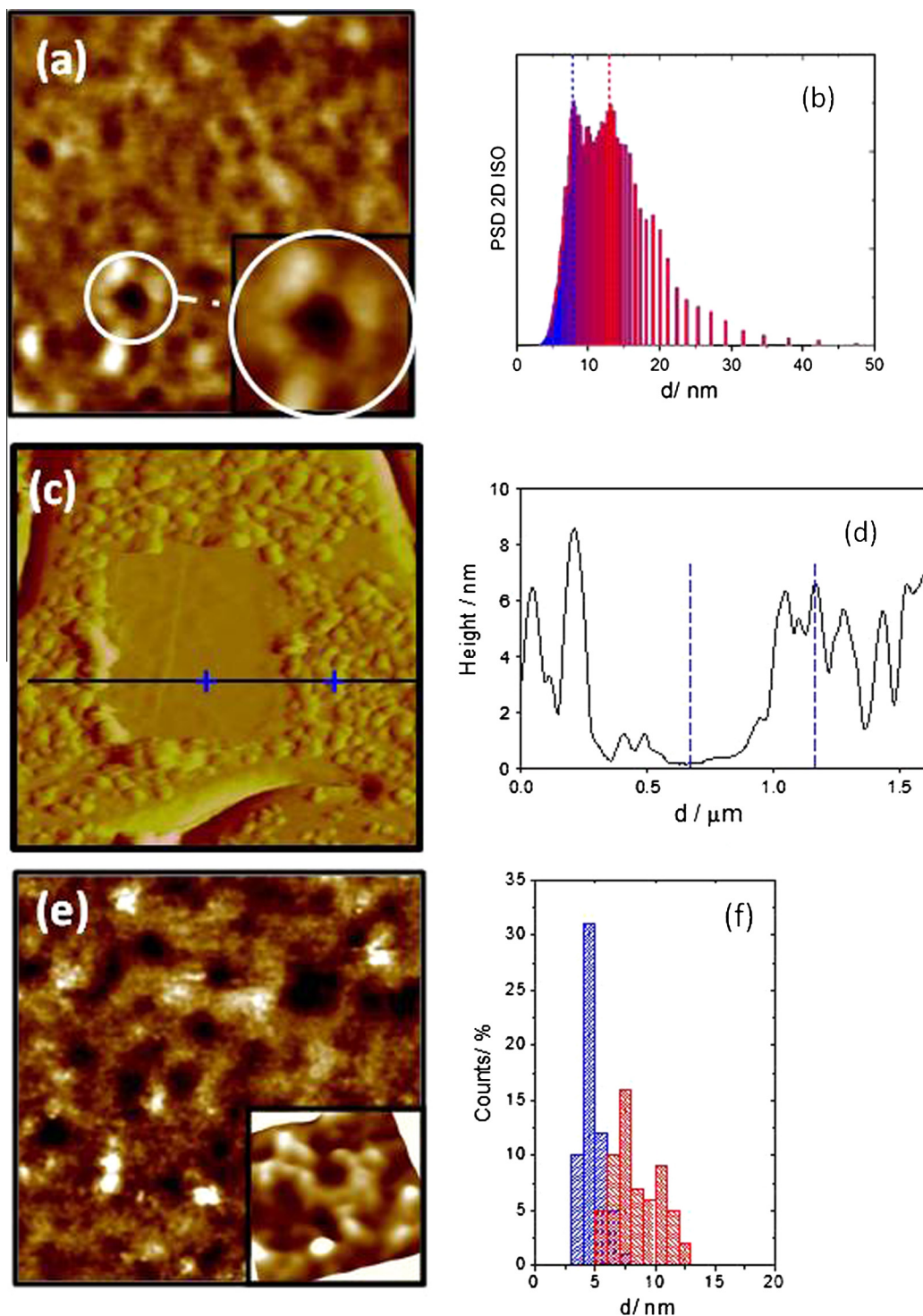


**Fig. 3.** (a)  $521 \times 521 \text{ nm}^2$  AFM image; inset:  $90 \times 90 \text{ nm}^2$  image showing in detail a single pore; (b) PSD of the  $350 \times 350 \text{ nm}^2$  image showing the two characteristic lengths. (c)  $2 \times 2 \mu\text{m}^2$  AFM image taken after repetitive scanning a preset area of the protein film (square window in the image). The thickness of the layer was measured by the cross section, (d) far from the border of the window to avoid computing the height of the accumulated material. (e)  $45 \times 45 \text{ nm}^2$  STM image; inset:  $40 \times 40 \text{ nm}^2$  3D STM image showing a single pore. (f) Statistical analysis of the size of the pores, red, and the flagellin units, blue, from STM images (60 units and pores were analyzed). (For interpretation of the references to color in this figure legend, the reader is referred to the web version of this article.)

primary structure on the Au surface leads to a secondary and more complex structure which includes the smaller pores  $\approx 7 \text{ nm}$  in average size originated by the contact of the rounded units of adjacent pores and also detected by STM (Fig. 6c).

The fact that the structure of the flagellin film on Au is similar to that formed on hydrophobic (silanized) surfaces [13] need to be

explained since the Au surface should be hydrophilic [32]. It has been observed that the contact angle of water on gold increases to  $60^\circ$  by carbonaceous contamination after the exposure of the substrate a few minutes to a laboratory environment [33]. Thus, this weakly adsorbed film turns hydrophobic the Au surface favoring the initial adsorption of flagellin by the D0 domain. However,

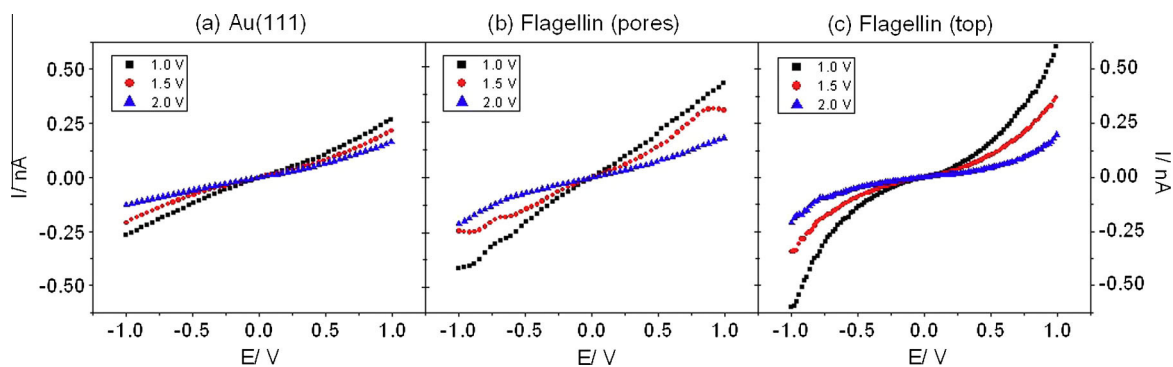


**Fig. 4.** STS curves corresponding to (a) Au(111) substrate; (b) tip positioned within the pores of the protein layer; (c) tip located on top of the rounded units of the protein layer.

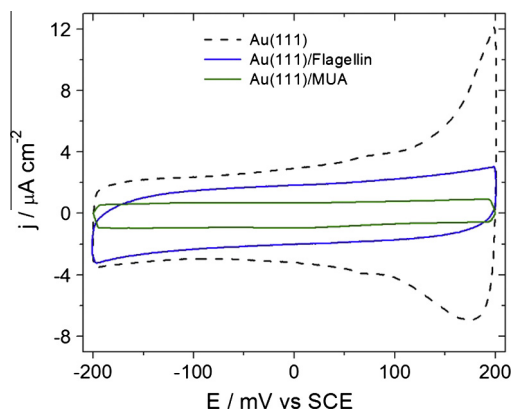


**Fig. 5.** Voltammograms in PB 10 mM, pH 7.3 of Au(111), Au(111) covered by flagellin (24 h of immersion in a 1:10 dissolution) and Au(111) covered by MUA.

the carbonaceous film should be finally displaced by the protein due to the stronger N-containing and carboxylate group interactions of aminoacids with the Au surface [34].

We have confirmed our model by adsorbing flagella, which expose the D2 and D3 subunits, on the Au surface. Fig. 7 shows an AFM image taken after the immersion of the Au surface into a suspension of flagella. Although there is a significant amount of flagella adsorbed on the gold surface, under our experimental conditions (24 h of immersion in the flagellar suspension and subsequent rinsing with PBS) the gold surface should appear totally covered by flagella. However, the filaments do not cover the entire surface, and, in many cases, they are adsorbed on other filaments. This suggests that the hydrophilic external part of the flagella with D2 and D3 exposed domains do not interact strongly with the Au surface.

In fact, adhesion force measurements of the flagella at various stages of solubilization were subsequently measured using a modified flagellar AFM tip [35]. Force–displacement curves between the modified probe and silicon substrate show that solubilized flagella have much better adhesion force as compared to as-extracted flagella.

Finally, we have explored the ability of the flagellin films to incorporate electrochemically active biomolecules. Thus, we have exploited the redox properties of the Fe(II)/Fe(III) redox couple of Cyt C since it is known that the direct electron transfer of nonspecifically adsorbed horse Cyt C on bare metal electrodes is hard to achieve [36–38] due to either different orientations and suppressed rotation [37] or partial denaturation [36,38]. First, the behavior of Cyt C directly adsorbed on our Au substrates was studied (Fig. 8a). A slight reduction in the double layer capacitance

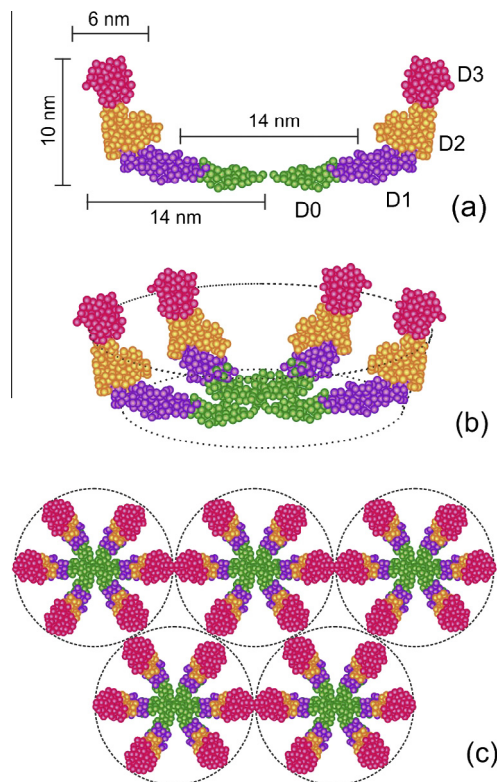


**Fig. 6.** Schemes showing (a) the conformation and the domains present in the adsorbed flagellin molecules and (b) the organization of the adsorbed flagellin in a cylindrical-like arrangement. Note that the two units located forwards are not drawn. (c) Top view of the possible arrangement of the cylinders that originates pores having different sizes.

indicates that some amount of Cyt C has been adsorbed on the Au surface. In agreement with previous studies concerning electrochemical response of horse Cyt C on gold electrodes, no voltammetric peaks related to the charge transfer of the Fe(II)/Fe(III) groups are observed. It is worth to mention that similar studies carried out using yeast Cyt C (YCC) demonstrated that the protein is able to adsorb on Au(111) in monolayer quantities [39], partly via thiolate linking between cysteine and gold [39,40]. Also, evidences of unfolding of YCC into structural forms preserving electron transfer reactivity have been reported [39]. In relation to our results, the slight decrease in the double layer capacitance after the immersion of the bare gold substrate in the Cyt C containing solution indicates that only a small amount of Cyt C has been adsorbed on the surface. Consequently, if a fraction of electrochemically active Cyt C is present on the Au surface, this amount

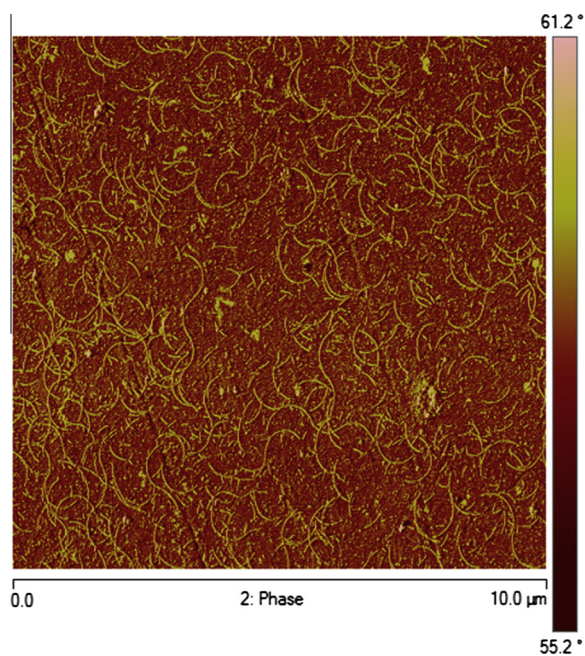


**Fig. 7.** AFM image (phase mode) of the flagellar filaments adsorbed on Au(111) ( $10\ \mu\text{m} \times 10\ \mu\text{m}$ ).

is too small to be detected in the voltammetric runs, i.e. the voltammetric peaks cannot emerge from the electrical double layer. In contrast, when the Cyt C is adsorbed on the thin flagellin film on the Au surface, a weak, although detectable, voltammetric signal corresponding to the Fe(II)/Fe(III) redox couple is recorded in the double layer region (Fig. 8b). This result agrees with previous voltammetric data showing that the Fe(II)/Fe(III) redox couple of the metalloprotein can be markedly improved when it is immobilized on self-assembled monolayers (SAMs) of MUA [38]. It should be noted that the porous flagellin film can allocate Cyt C as the diameter of this molecule is  $\approx 4\text{--}5\ \text{nm}$  [41] and the pores in the flagellin films are  $\approx 14\ \text{nm}$  in size (Fig. 2). Therefore, we expect a population of Cyt C trapped in the outer hydrophilic part of the pores or adsorbed on top of the thin film by weak interactions with residues of the external flagellin domains. In particular the negatively charged carboxyl regions of the flagellin molecule can interact with the positively charged lysine-rich domain around a heme exposed left [42] as proposed for Cyt C immobilized on MUA SAMs [43].

The Cyt C could be able to transfer electrons to the Au surface by tunneling through the thin protein film as occurs for these molecules in SAMs [38,44]. The redox potential of the immobilized Cyt C species estimated from the voltammogram is  $E_r = -0.01\ \text{V}$ , close to  $E_r = 0.01\ \text{V}$  reported in the literature [45]. Values of  $E_r$  diverging from  $0.02\ \text{V}$  have been assigned to configurations that in some way do not favor the electron transfer between the surface and the protein [38]. Similar potential shifts towards more negative values had been observed on negative charged SAM-modified gold electrodes [36], suggesting that, in our case, the negative values of  $E_r$  could be related to the carboxyl rich regions in the flagellin close to the heme pocket of Cyt C that make more difficult the charge transfer process. On the other hand, the peak separation gives  $E_p = 0.06\ \text{V}$ , the value expected for an ideal one-electron transfer reaction [46]. This figure suggests that there is no marked constraints to the charge transfer process for the Cyt C adsorbed on the flagellin film, in contrast to that observed for Cyt C directly adsorbed on the Au surface [36–38].

We have also prepared flagellin films of at least  $60\ \text{nm}$  in thickness by drop casting. The XPS analysis of these thick protein layers

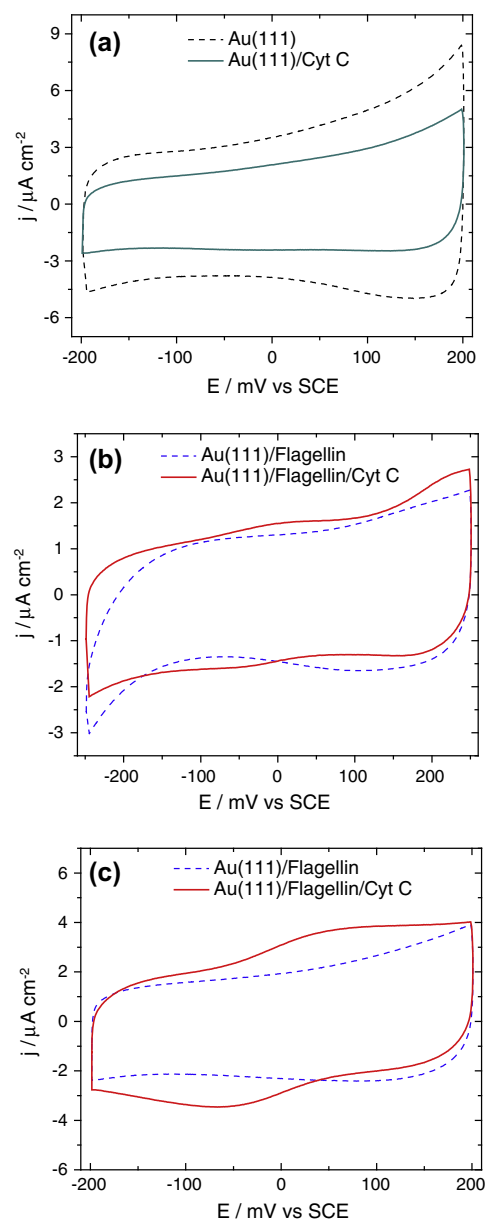


**Fig. 8.** Voltammograms in PB  $10\ \text{mM}$ , pH 7.3,  $100\ \text{mV s}^{-1}$ . (a) Au(111) and Au(111) covered by Cyt C (b) Au(111) covered by flagellin (24 h of immersion in a 1:10 dissolution, thin layer) and Cyt C (c) Au(111) covered by flagellin (drop casting, thick layer) and Cyt C.

(Fig. 9a) are similar to that recorded for the assembled layer of flagellin (Fig. 1a). As expected, AFM imaging shows that the topography of this thick film has a different structure when compared to the features of the assembled flagellin. In fact, the features of the thick films are consistent with a multilayered arrangement formed by randomly ordered granules having about  $100\text{--}200\ \text{nm}$  in size (Fig. 9b). The voltammograms recorded after Cyt C adsorption on these films (Fig. 8c) reveal that the charge associated to the Fe(II)/Fe(III) redox couple is about 10-fold larger than that corresponding to the thin layer of flagellin (Fig. 8b). In this case direct tunneling from the Cyt C to the Au surface cannot be the predominant mechanism. In fact, it should be expected that Fe(II)/Fe(III) species should be electrochemical silent for redox center-substrate separation larger than  $1\ \text{nm}$  since the probability of direct tunneling should decay exponentially with the distance between the heme group and the surface of the electrode [47,48]. On the other hand, the peak to peak separation for the thick layer is about twice

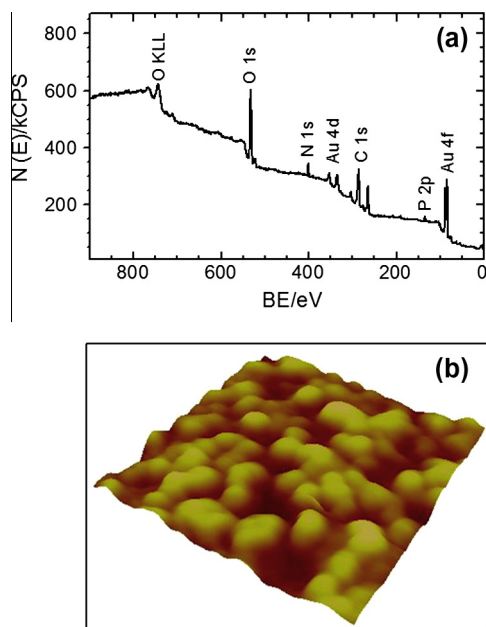


**Fig. 9.** (a) XPS spectrum of the thick layer of flagellin prepared by drop casting. (b) AFM image (3D, topographic mode,  $1.1 \times 1.1 \mu\text{m}^2$ ) of the film.

(0.10 V) the value obtained for the thin layer, which is consistent with an increase in the irreversibility of the reaction as the thickness of the adsorbed layer increases. Considering that the number of ions and water molecules trapped in the porous film is high (Fig. 4a) we can discard a significant change in the electrolyte resistance with the increase in the flagellin film thickness. Furthermore, the larger charge values and the more irreversible electrochemical response of the heme group in the thicker protein films (Fig. 8c) suggests that the direct tunneling from Cyt C to the Au surface through the protein layer cannot be the predominant mechanism since it expects that the Fe(II)/Fe(III) species should be electrochemically silent for redox-substrate separation larger than 1 nm. Thus, we speculate that a delocalized electron transfer mechanism associated directly to the flagellin units is involved in the charge transfer reactions, as it has been proposed for the conductivity of flagellar filaments [49,50].

#### 4. Conclusions

The adsorption of flagellin on Au(111) has been studied by AFM, STM, SPR and electrochemical techniques. The results show that flagellin monomers spontaneously self-assemble forming a monolayer protein film bounded to the Au surface by the more hydrophobic subunit and exposed to the environment the hydrophilic subunit. The assembly of the protein on the surface can be modeled as cylindrical-like structures containing 4–6 units of flagellin. The films are conductive and allow allocation of electrochemically active Cyt C. The self-assembled films could be used as biological platforms to build 3D complex molecular structures on planar metal surfaces and to functionalize metal nanoparticles.

#### Acknowledgments

The authors acknowledge to CONICET, UNLP (11/X665), ANPCyT (PICT 2010-1779, PICT 2010-2554) and Project CTQ2011-24784, MINECO, Spain. A.G.O., A.G.M and D.E.P. acknowledge the fellowships from Fundación Cajacanarias, CONICET and ANPCyT, respectively.

#### References

- [1] Y.H. Tan, M. Liu, B. Nolting, J.G. Go, J. Gervay-Hague, G.-Y. Liu, *ACS Nano* 2 (2008) 2374–2384.
- [2] H. Uedaira, H. Morii, M. Ishimura, H. Taniguchi, K. Namba, F. Vonderviszt, *FEBS Lett.* 445 (1999) 126–130.
- [3] A. Muskotal, C. Seregelyes, A. Sebestyén, F. Vonderviszt, *J. Mol. Biol.* 403 (2010) 607–615.
- [4] V. Szabo, A. Muskotal, B. Toth, M.D. Mihovilovic, F. Vonderviszt, *PLoS ONE* 6 (2011) e25388.
- [5] S.A. Beatson, T. Minamino, M.J. Pallen, *Trends Microbiol.* 14 (2006) 151–155.
- [6] S. Kurunczi, R. Horvath, Y.-P. Yeh, A. Muskotal, A. Sebestyén, F. Vonderviszt, *J.J. Ramsden, J. Chem. Phys.* 130 (2009).
- [7] Á. Klein, B. Tóth, H. Jankovics, A. Muskotal, F. Vonderviszt, *Protein Eng. Des. Sel.* 25 (2012) 153–157.
- [8] R. Brunner, E. Jensen-Jarolim, I. Pali-Schöll, *Immunol. Lett.* 128 (2010) 29–35.
- [9] J.W. Huleatt, A.R. Jacobs, J. Tang, P. Desai, E.B. Kopp, Y. Huang, L. Song, V. Nakaar, T.J. Powell, *Vaccine* 25 (2007) 763–775.
- [10] D. Kozlova, V. Sokolova, M. Zhong, E. Zhang, J. Yang, W. Li, Y. Yang, J. Buer, A. Westendorf, M. Epple, H. Yan, *Viro. Sin.* 29 (2014) 33–39.
- [11] H.H. Salman, J.M. Irache, C. Gamazo, *Vaccine* 27 (2009) 4784–4790.
- [12] M. Shah, V.D. Badwaik, R. Dakshinamurthy, *J. Nanosci. Nanotechnol.* 14 (2014) 344–362.
- [13] N. Kovacs, D. Patko, N. Orgovan, S. Kurunczi, J.J. Ramsden, F. Vonderviszt, R. Horvath, *Anal. Chem.* 85 (2013) 5382–5389.
- [14] Y. Hiriart, A. Errea, D.G. Maciel, J.C. Lopez, M. Rumbo, *World J. Microbiol. Biotechnol.* 28 (2012) 15–21.
- [15] W.M. Albers, I.V. Lundin, in: S. Carrara (Ed.), *Nano-Bio-Sensing*, first ed., Springer, 2010 (chapter 4).
- [16] L. Caprile, A. Cossaro, E. Falletta, C. Della Pina, O. Cavalleri, R. Rolandi, S. Terreni, R. Ferrando, M. Rossi, L. Floreano, M. Canepa, *Nanoscale* 4 (2012) 7727–7734.
- [17] O. Cavalleri, G. Gonella, S. Terreni, M. Vignolo, L. Floreano, A. Morgante, M. Canepa, R. Rolandi, *Phys. Chem. Chem. Phys.* 6 (2004) 4042–4046.
- [18] S.K. Das, C. Dickinson, F. Lafir, D.F. Brougham, E. Marsili, *Green Chem.* 14 (2012) 1322–1334.
- [19] K. Kelly-Wintenberg, S.L. South, T.C. Montie, *J. Bacteriol.* 175 (1993) 2458–2461.
- [20] Y.A. Gorby, S. Yanina, J.S. McLean, K.M. Rosso, D. Moyles, A. Dohnalkova, T.J. Beveridge, I.S. Chang, B.H. Kim, K.S. Kim, D.E. Cullley, S.B. Reed, M.F. Romine, D.A. Saffarini, E.A. Hill, L. Shi, D.A. Elias, D.W. Kennedy, G. Pinchuk, K. Watanabe, S.I. Ishii, B. Logan, K.H. Nealson, J.K. Fredrickson, *Proc. Natl. Acad. Sci.* 103 (2006) 11358–11363.
- [21] N.S. Wigginton, K.M. Rosso, B.H. Lower, L. Shi, M.F. Hochella Jr., *Geochim. Cosmochim. Acta* 71 (2007) 543–555.
- [22] R. Guckenberger, M. Heim, G. Cevc, H. Knapp, W. Wiegand, A. Hillebrand, *Science* 266 (1994) 1538–1540.
- [23] J.P. Busalmen, A. Berna, J.M. Feliu, *Langmuir* 23 (2007) 6459–6466.
- [24] S.E. Moulton, J.N. Barisci, A. Bath, R. Stella, G.G. Wallace, *Electrochim. Acta* 49 (2004) 4223–4230.
- [25] K. Yonekura, S. Maki-Yonekura, K. Namba, *Nature* 424 (2003) 643–650.
- [26] K. Yonekura, S. Maki-Yonekura, K. Namba, *Res. Microbiol.* 153 (2002) 191–197.
- [27] S.A. Beatson, T. Minamino, M.J. Pallen, *Trends Microbiol.* 14 (2006) 151–155.
- [28] F. Vonderviszt, S. Kanto, S.-I. Aizawa, K. Namba, *J. Mol. Biol.* 209 (1989) 127–133.
- [29] A.V. Verde, J.M. Acres, J.K. Maranas, *Biomacromolecules* 10 (2009) 2118–2128.
- [30] J. Feng, R.B. Pandey, R.J. Berry, B.L. Farmer, R.R. Naik, H. Heinz, *Soft Matter* 7 (2011) 2113–2120.
- [31] UniProt and <http://www.uniprot.org/>.
- [32] T. Smith, *J. Colloid Interface Sci.* 75 (1980) 51–55.
- [33] S. Gourianova, N. Willenbacher, M. Kutschera, *Langmuir* 21 (2005) 5429–5438.
- [34] A.A. Ooka, K.A. Kuhar, N. Cho, R.L. Garrell, *Biospectroscopy* 5 (1999) 9–17.
- [35] S. Ramaswamy, D. Suresh, H. Bathula, O. Mahapatra, K.D. Arunachalam, C. Gopalakrishnan, *J. Adv. Microsc. Res.* 8 (2013) 163–170.
- [36] X. Chen, R. Ferrigno, J. Yang, G.M. Whitesides, *Langmuir* 18 (2002) 7009–7015.
- [37] S. Lin, X. Jiang, L. Wang, G. Li, L. Guo, J. Phys. Chem. C 116 (2011) 637–642.
- [38] T.D.F. Paulo, T.P. de Sousa, D.S. de Abreu, N.H. Felício, P.V. Bernhardt, L.G. de F. Lopes, E.H.S. Sousa, I.C.N. Diógenes, *J. Phys. Chem. B* 117 (2013) 8673–8680.
- [39] A.G. Hansen, A. Boisen, J.U. Nielsen, H. Wackerbarth, I. Chorkendorff, J.E.T. Andersen, J. Zhang, J. Ulstrup, *Langmuir* 19 (2003) 3419–3427.
- [40] C. Toccafondi, M. Prato, G. Maidecchi, A. Penco, F. Bisio, O. Cavalleri, M. Canepa, *J. Colloid Interface Sci.* 364 (2011) 125–132.
- [41] G.V. Louie, G.D. Brayer, *J. Mol. Biol.* 214 (1990) 527–555.
- [42] J. Xu, E.F. Bowden, *J. Am. Chem. Soc.* 128 (2006) 6813–6822.
- [43] R.A. Clark, E.F. Bowden, *Langmuir* 13 (1997) 559–565.
- [44] K. Nakano, T. Yoshitake, Y. Yamashita, E.F. Bowden, *Langmuir* 23 (2007) 6270–6275.
- [45] G.R. Moore, G.W. Pettigrew, *Cytochrome C: Evolution, Structural and Physicochemical Aspects*, Springer-Verlag, 1990.
- [46] J. Wang, *Analytical Electrochemistry*, Wiley, 2006.
- [47] C.C. Moser, J.M. Keske, K. Warncke, R.S. Farid, P.L. Dutton, *Nature* 355 (1992) 796–802.
- [48] C.C. Page, C.C. Moser, X. Chen, P.L. Dutton, *Nature* 402 (1999) 47–52.
- [49] N.S. Malvankar, M. Vargas, K.P. Nevin, A.E. Franks, C. Leang, B.-C. Kim, K. Inoue, T. Mester, S.F. Covalla, J.P. Johnson, V.M. Rotello, M.T. Tuominen, D.R. Lovley, *Nat Nano* 6 (2011) 573–579.
- [50] J.P. Veazey, G. Reguera, S.H. Tessmer, *Phys. Rev. E* 84 (2011) 060901.